Propagation Characteristics of Picosecond Electrical Pulses on a Periodically Loaded Coplanar Waveguide

Chester Shu, Xu Wu, Edward S. Yang, *Senior Member, IEEE*, X.-C. Zhang, and David H. Auston, *Fellow, IEEE*

Abstract—**We have developed a theoretical model to investigate the propagation characteristics of picosecond electrical pulses on a coplanar waveguide capacitively coupled to periodically spaced sampling channels. Various factors which affect the signal waveform were analyzed in both the frequency and the time domain. The results showed that in addition to modal dispersion, conductor loss, and radiation loss of the electrical signals, multiple reflections among the sampling gaps constitute another feature of the signal transfer along the waveguide. We have measured the picosecond pulse dispersion using the optoelectronic correlation technique. The experimental data were compared with the theoretical results.**

I. Introduction

RECENTLY, the generation and detection of ultrashort electrical pulses with femtosecond lasers [1], [2] have received much attention in the characterization of materials and high-speed devices [3]–[5]. It is also of great interest to study the behavior of these ultrashort pulses as they propagate along a transmission line. Some theoretical work has been done on this subject [6]–[8]. The comparison of theory with experimental results obtained from electro-optic sampling [9], correlation sampling [10], and sampling oscilloscope measurements [11] has shown a number of similarities on the main features of the dispersed pulse shapes. In this work, we concentrated on the studies of pulses propagating on a coplanar waveguide periodically loaded with sampling channels. A very similar structure has been commonly used for the experimental determination of picosecond pulse dispersion [12], [13]; however, the influence of multiple reflections among the sampling gaps has not been addressed. The device structure also has a potential application in broad-band optoelectronic time division demultiplexing [14]. Therefore, it is important to develop a theoretical model to predict the propagation characteristics of the signal pulses. We will present a model which takes into account the effect of multiple reflections. The calculated pulse waveforms at various sampling distances showed an agreement with the experimental observations.

Manuscript received June 18, 1990; revised January 22, 1991. This work was supported by the National Science Foundation through the Center for Telecommunications Research at Columbia University.

The authors are with the Department of Electrical Engineering, Columbia University, New York, NY 10027.

IEEE Log Number 9144281.

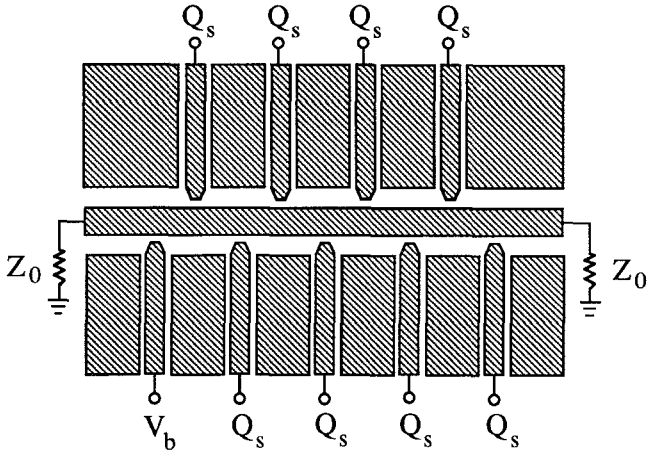

Fig. 1. Top view of the periodically loaded coplanar waveguide.

II. Theory

We consider a coplanar waveguide capacitively coupled to periodically spaced sampling channels (Fig. 1). A substrate material with picosecond photoconductive response is assumed. Suppose an electrical pulse is launched into the waveguide by applying an optical pulse at the first channel gap, which is biased with dc. The signal which has propagated for a certain distance and then been sampled by optoelectronic correlation will be calculated.

The initial pulse, $V(0,t)$, at zero propagation distance has a fast rise time determined by the laser pulse width and the time constant of the circuit. The fall time, which is usually longer, depends mostly on the decay of the photogenerated carriers. In order to compute the sampled waveforms, it is more convenient to work in the frequency domain and then convert the results back to the time domain by Fourier transform. The sampled pulse in the frequency domain is given by

$$S(L,f) = V(0,f) \times T(L,f) \times V'(f) \qquad (1)$$

where L is the pulse propagation distance, $V(0,f)$ is the Fourier transform of the initial pulse, $T(L,f)$ is the

0018-9480/91/0600-0930$01.00 ©1991 IEEE

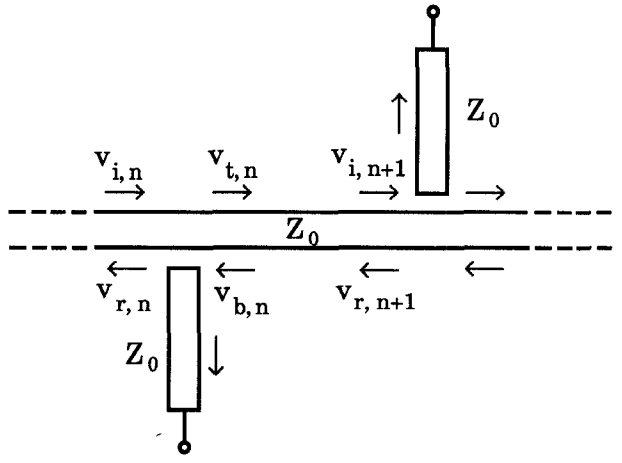

Fig. 2. Electrodes showing amplitudes of traveling waves at two adjacent channels.

transfer function determined by the material and the geometry of the waveguide, and $V'(f)$ is the frequency response of the sampling gap.

Our goal is to find an expression for the transfer function of the structure in Fig. 1. The sampled waveform at each channel can then be evaluated using (1). Fig. 2 shows the electrodes of two adjacent channels with the symbols $v_{i,j}$ representing the amplitudes of the traveling waves at a particular position. Applying circuit laws to an arbitrary channel (denoted by n), we obtain

$$v_{i,n} + v_{r,n} = v_{t,n} + v_{b,n} \tag{2}$$

$$\frac{v_{i,n} - v_{r,n}}{Z_0} = \frac{v_{t,n} - v_{b,n}}{Z_0} + \frac{v_{t,n} + v_{b,n}}{Z_0 - \dfrac{j}{2\pi fC}} \tag{3}$$

where $j^2 = -1$, Z_0 is the characteristic impedance of the waveguide, C is the coupling capacitance between the waveguide and a side channel, and the voltage amplitudes are defined in Fig. 2. For simplicity, the dark conductance of the gaps has been neglected. This is justified for high-resistivity semi-insulating substrates.

Combining (2) and (3) and rearranging, we obtain

$$\begin{pmatrix} v_{t,n} \\ v_{b,n} \end{pmatrix} = \begin{pmatrix} 1-\kappa & -\kappa \\ \kappa & 1+\kappa \end{pmatrix} \begin{pmatrix} v_{i,n} \\ v_{r,n} \end{pmatrix} \tag{4}$$

with

$$\kappa = \frac{Z_0}{2\left(Z_0 - \dfrac{j}{2\pi fC}\right)}. \tag{5}$$

The signals at the nth channel are related to those at the $(n+1)$th channel by the propagation factor $\gamma(f)$, where

$$\gamma(f) = \alpha(f) + j\beta(f). \tag{6}$$

Here $\alpha(f)$ and $\beta(f)$ are the attenuation factor and the phase factor of propagation, respectively. Thus,

$$\begin{pmatrix} v_{i,n+1} \\ v_{r,n+1} \end{pmatrix} = \begin{pmatrix} (1-\kappa)e^{-\gamma(f)l} & -\kappa e^{-\gamma(f)l} \\ \kappa e^{\gamma(f)l} & (1+\kappa)e^{\gamma(f)l} \end{pmatrix} \begin{pmatrix} v_{i,n} \\ v_{r,n} \end{pmatrix} \tag{7}$$

where l is the separation between two channels. Equation (7) shows a recursive relation for the signals at adjacent channels for $n = 2$ to $m-1$, where m is the total number of channels in the structure. By applying (7) repeatedly, we obtain

$$\begin{pmatrix} v_{t,n+1} \\ v_{r,n+1} \end{pmatrix} = M^{n-1} \begin{pmatrix} v_{i,2} \\ v_{r,2} \end{pmatrix} \tag{8}$$

where the matrix

$$M = \begin{pmatrix} (1-\kappa)e^{-\gamma(f)l} & -\kappa e^{-\gamma(f)l} \\ \kappa e^{\gamma(f)l} & (1+\kappa)e^{\gamma(f)l} \end{pmatrix}$$

can be diagonalized in the eigenspace spanned by its eigenvectors $\tilde{A}_1$ and $\tilde{A}_2$, with

$$\tilde{A}_1 = \begin{pmatrix} 2\kappa e^{-\gamma(f)l} \\ (1-\kappa)e^{-\gamma(f)l} - (1+\kappa)e^{\gamma(f)l} - \sqrt{\zeta} \end{pmatrix} \tag{9a}$$

$$\tilde{A}_2 = \begin{pmatrix} 2\kappa e^{-\gamma(f)l} \\ (1-\kappa)e^{-\gamma(f)l} - (1+\kappa)e^{\gamma(f)l} + \sqrt{\zeta} \end{pmatrix} \tag{9b}$$

and

$$\zeta = \left[(1-\kappa)e^{-\gamma(f)l} + (1+\kappa)e^{\gamma(f)l}\right]^2 - 4. \tag{9c}$$

The corresponding eigenvalues are

$$\lambda_{1,2} = \frac{(1-\kappa)e^{-\gamma(f)l} + (1+\kappa)e^{\gamma(f)l} \pm \sqrt{\zeta}}{2} \tag{10}$$

respectively. Let us denote

$$\begin{pmatrix} a_n & b_n \\ c_n & d_n \end{pmatrix} = M^n = P \begin{pmatrix} \lambda_1 & 0 \\ 0 & \lambda_2 \end{pmatrix}^n P^{-1} \tag{11}$$

where P is the 2×2 matrix composed of the eigenvectors $\tilde{A}_1$ and $\tilde{A}_2$. With a proper termination on the coplanar waveguide, there is no signal reflection back to the last (mth) channel. Applying straightforward voltage and current relations and combining them, we have

$$\kappa v_{i,m} + (\kappa+1)v_{r,m} = 0. \tag{12}$$

Replacing $n+1$ by m in (8) and substituting it into (12), we obtain a relation between $v_{i,2}$ and $v_{r,2}$:

$$\left[\kappa a_{m-2} + (\kappa+1)c_{m-2}\right]v_{i,2} + \left[\kappa b_{m-2} + (\kappa+1)d_{m-2}\right]v_{r,2} = 0. \tag{13}$$

Equation (8) can then be rewritten as

$$\begin{pmatrix} v_{i,n+1} \\ v_{r,n+1} \end{pmatrix} = M^{n-1} \begin{pmatrix} 1 \\ -\dfrac{\kappa a_{m-2} + (\kappa+1)c_{m-2}}{\kappa b_{m-2} + (\kappa+1)d_{m-2}} \end{pmatrix} e^{-\gamma(f)l} v_{t,1} \tag{14}$$

where we have used the relation $v_{i,2} = e^{-\gamma(f)l} v_{t,1}$, with $v_{t,1}$ being the input electrical signal at the first channel. The transfer function

$$T(L,f) = \frac{v_{i,n+1} + v_{r,n+1}}{v_{t,1}}$$

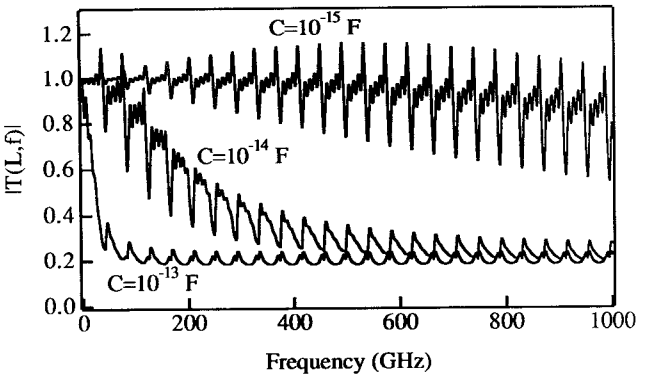

Fig. 3. Frequency dependence of the amplitude of transfer function caused by multiple reflections of signals among the sampling channels.

where $L = nl$, is given by

$$T(L,f) = e^{-\gamma(f)l} \cdot \left[a_{n-1} + c_{n-1} - (b_{n-1} + d_{n-1}) \frac{\kappa a_{m-2} + (\kappa+1) c_{m-2}}{\kappa b_{m-2} + (\kappa+1) d_{m-2}} \right]. \quad (15)$$

The frequency dependence of the transfer function is determined by the propagation factor $\gamma(f)$ and the multiple reflections through $\kappa = \kappa(f)$ in (5). For dc input, $\kappa(f) = 0$ and (15) reduces to $T(L,f) = 1$. At very high frequencies, κ approaches $1/2$ and $T(L,f)$ will reach a limiting value determined by the propagation distance and the total number of channels in the structure.

Fig. 3 shows the frequency spectrum of $|T(L,f)|$ with the coupling capacitance as a parameter. The curves are plotted for the case of $m = 9$, relative permittivity = 13.1, propagation distance = 4 mm, and a spacing of 1 mm between adjacent channels. Attenuation and dispersion caused by the frequency dependence of the propagation factor have been neglected for the moment. There are a number of interesting features in the plot. Each curve is bounded by two envelopes. These are the maxima and minima of the interference patterns generated by the multiple reflections. As an illustration, consider the simple case of two gaps in the structure. Suppose F is the amplitude at a particular frequency of the incident signal and R_1 and R_2 are the reflection coefficients. The maximum amplitude, F_+, will be given by the constructive interference of the multiple reflections:

$$F_+ = F + F(R_1R_2)\exp(-j\beta 2l) + F(R_1R_2)^2 \cdot \exp(-j\beta 4l) + \cdots = F/(1 - R_1R_2). \quad (16)$$

Similarly, the minima correspond to destructive interference of the multiple reflections.

$$F_- = F - F(R_1R_2)\exp(-j\beta 2l) + F(R_1R_2)^2 \cdot \exp(-j\beta 4l) - \cdots = F/(1 + R_1R_2). \quad (17)$$

Thus, the ratio of the maximum and minimum amplitudes provides information on the reflection coefficients at different frequencies. In the case where the signal attenuation caused by the conductor loss, the dielectric loss, and the radiation loss cannot be neglected, (16) and (17) have to be modified and they can be used to derive the loss spectrum of the signal transfer along the waveguide.

The spacing of frequency modes can also be obtained from

$$\Delta\nu = \frac{c}{\sqrt{\epsilon_r}\, 2l} \quad (18)$$

where c is the velocity of light in free space and ϵ_r is the relative permittivity. For $\epsilon_r = 13.1$ and $l = 1$ mm, $\Delta\nu$ is equal to 41.4 GHz, consistent with the results in Fig. 3. The curves also show fine structures of oscillations at ~ 10 GHz. These are caused by resonating modes at longer wavelengths, which satisfy the boundary conditions from the end channels 4 mm apart.

When the capacitance is large, $|T(L,f)|$ decreases rapidly with increasing frequency and it saturates at a value depending on L and the total number of channels. As the capacitance becomes smaller, $|T(L,f)|$ decreases slowly with increasing frequency because of weaker signal reflections in the structure. However, at sufficiently high frequencies, all the curves in Fig. 3 will eventually merge.

In the following, the frequency dependence of the propagation factor is taken into consideration. The phase factor $\beta(f)$ is given by

$$\beta(f) = \frac{2\pi f \sqrt{\epsilon_{\text{eff}}(f)}}{c}. \quad (19)$$

The effective permittivity, $\epsilon_{\text{eff}}(f)$, depends on frequency and causes dispersion of signals on the waveguide. Part of the traveling wave propagates in free space on the surface of the material rather than totally inside the substrate, resulting in a smaller effective permittivity. This effect is stronger for lower frequency components, which will then have higher velocities of propagation. In the model, we used the following dispersion formula, derived in [15] and subsequently modified for coplanar structures in [8]:

$$\sqrt{\epsilon_{\text{eff}}(f)} = \frac{\sqrt{\epsilon_r} - \sqrt{\epsilon_{\text{eff}}(0)}}{1 + aF^{-b}} + \sqrt{\epsilon_{\text{eff}}(0)} \quad (20)$$

where $\epsilon_{\text{eff}}(0)$ is the effective permittivity at the quasi-static limit [16], $F = f/f_{\text{TE}}$ with $f_{\text{TE}} = c/[4h(\epsilon_r - 1)^{1/2}$ being the cutoff frequency for the lowest order TE mode, h is the substrate thickness, and a and b are dimensionless parameters depending on the geometry of the waveguide. Fig. 4 plots the frequency dependence of $\sqrt{\epsilon_{\text{eff}}(f)}$ with $f_{\text{TE}} = 34$ GHz, $\epsilon_r = 13.1$, $a = 180$, and $b = 1.7$. These values will be used in the calculations in Section IV for comparison with the experimental results. One should notice that the modal dispersion affects only the phase factor, whereas the multiple reflections modify both the magnitude and the phase of the transfer function.

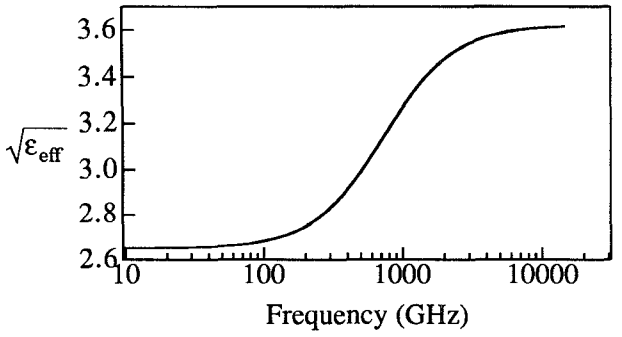

Fig. 4. Frequency dependence of the square root of effective permittivity.

Attenuation of signals in the coplanar waveguide caused by frequency-dependent conductor loss is given by [16]

$$\alpha_c = 4.88\times10^{-4} R_S(f)\epsilon_{\text{eff}} Z_0 \cdot \frac{P'}{\pi W}\cdot\left(1+\frac{S}{W}\right) \cdot\left\{\frac{\frac{1.25}{\pi}\ln\frac{4\pi S}{t}+1+\frac{1.25t}{\pi S}}{\left[2+\frac{S}{W}-\frac{1.25t}{\pi W}\left(1+\ln\frac{4\pi S}{t}\right)\right]^2}\right\} \quad \text{dB/unit length} \tag{21}$$

where $R_S(f)$ is the surface resistivity of the metal and has a square root dependence on frequency, W is the width of the center strip, S is the spacing between the strip and the ground planes, P' is a dimensionless parameter depending on W and S, and t is the metal thickness.

At 10 GHz, the signal will have an attenuation of 0.15 dB/mm in our case. This value is relatively large for the coplanar waveguide owing to the use of thin metal layer and narrow center strip. The signal attenuation caused by the dc conductor loss is relatively small, and has been neglected in our calculation.

Another cause of attenuation is the radiation of wave in the substrate upon propagation [17]. The loss factor is given by

$$\alpha_r = \frac{58.7}{K'K}\frac{(1-1/\epsilon_r)^2}{\sqrt{1+1/\epsilon_r}}\frac{(W+2S)^2}{\lambda_d^3} \quad \text{dB/unit length} \tag{22}$$

where K' and K are elliptical integrals of the first and second kind and are functions of W and S, and λ_d is the wavelength in the dielectric. In our case, α_r is calculated to be $2.38\times10^{-34} f^3$ dB/mm.

The frequency dependence of the conductor loss, the radiation loss, and their sum are plotted in Fig. 5. At relatively low frequencies, the conductor loss is dominant. As the frequency becomes higher, the radiation loss increases substantially because of the cubic dependence on frequency. The crossover point for the losses is at 132 GHz. Attenuation resulting from dielectric loss in the substrate is comparatively unimportant. Thus, the effect has been omitted in the calculation.

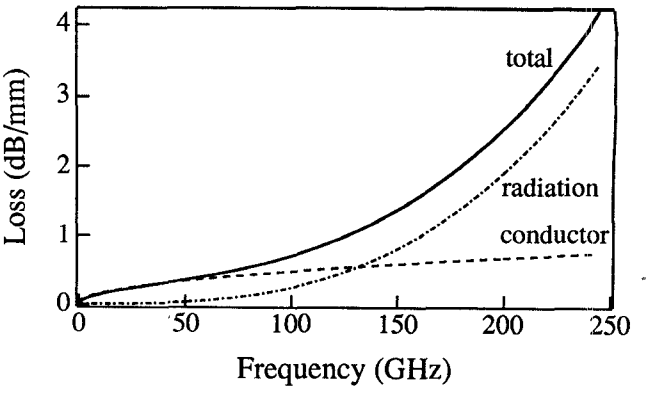

Fig. 5. Calculated conductor loss, radiation loss, and the total loss on the coplanar waveguide as a function of frequency.

III. Experiment

The device structure was prepared on an undoped semi-insulating GaAs wafer. The coplanar waveguide was formed by Au–Ge/Ni metallization using photolithography and the standard lift-off technique. Subsequent rapid thermal annealing at 400 °C for 20 s turned the metal into an alloyed ohmic contact. The sample was then implanted with 200 keV protons at an ion dose of $7\times10^{14}/\text{cm}^2$ and a beam current of 50 μA. Following the implantation, it was wire-bonded for external electrical connections and was mounted on a sample holder for measurements. The structure consists of a coplanar waveguide of width 50 μm loaded with nine channels (Fig. 1). The width and the spacing of the channels are 25 μm and 1000 μm, respectively. The waveguide and the channels are designed to have a 50 Ω characteristic impedance. At the end of each channel is an 8 μm photoconductive gap for either the generation or the detection of ultrafast electrical signals.

For the measurement, we used the standard "pump and probe" technique as described in [1]. The optical source was a balanced colliding pulse mode-locked (CPM) Rh 6G dye laser at a center wavelength of 620 nm. The pulse width (FWHM) was 60 fs and the repetition rate was 100 MHz with an output energy of 0.2 nJ per pulse. A beam splitter was used to split the laser beam into two paths. The pump beam was modulated by a chopper and was focused on the photoconductive gap at the first channel, which was biased at 3 V. An ultrashort electrical pulse was then launched into the coplanar waveguide transmission line. The probe beam, variably delayed, was focused on a downstream photoconductive gap to provide gating of the propagated signal. Total electrical charge through the sampling channel was measured by a lock-in amplifier. The output was plotted as a function of the delay time between the two synchronized laser beams.

IV. Results and Discussions

To determine the system response, an autocorrelation measurement was carried out on an optoelectronic switch fabricated together with the waveguide. A response time (FWHM) of 1.4 ps was obtained. Next, the signal on the

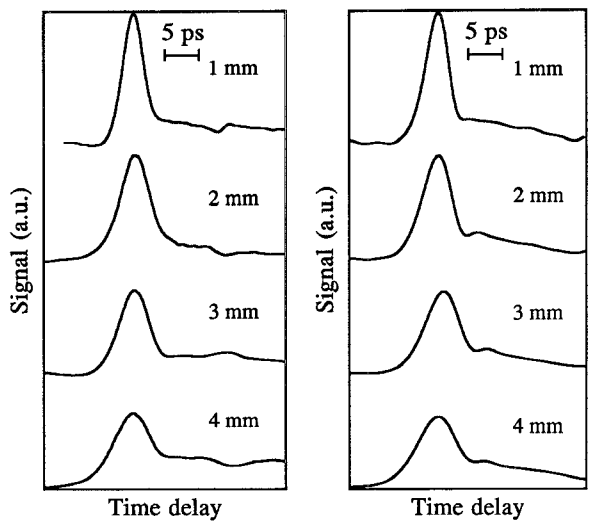

Fig. 6. Correlation curves at a propagation distance of 1 mm to 4 mm: (a) measured results; (b) calculated results.

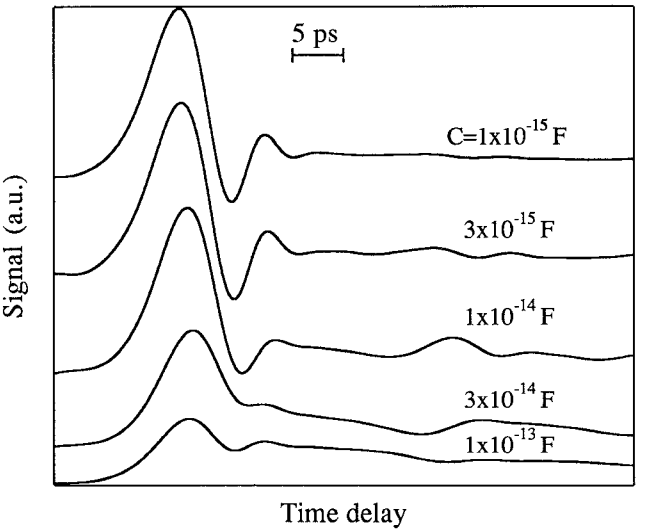

Fig. 7. Calculated correlation curves at 4 mm propagation distance. The coupling capacitance is used as a parameter.

coplanar waveguide was sampled at a propagation distance of 1 mm to 4 mm, i.e., from the second channel to the fifth channel. The correlation results are shown in Fig. 6(a). The horizontal axes of the curves have been shifted for a clear comparison. The rising front is related to the photoconductive response of the sampling gap and the dispersion on the rising edge of the original pulse signal. The trailing part is mainly determined by a convolution of the response of the pulse generating gap and the propagation characteristics of the waveguide. Asymmetries of the waveforms are due to a combination of factors. One main cause is the circuit response in the discharging of the pulse generating gap and the charging of the sampling gap [7]. In addition, modal dispersion, skin depth loss, radiation loss, and multiple reflections of the signals also play an important role in the resulting asymmetry.

Fig. 6(b) depicts the correlation waveforms calculated from (1). The input signal has a rise time of 0.5 ps, a primary decay time of 0.8 ps with a weight factor of 0.95, and a secondary decay time of 100 ps with a weight factor of 0.05. The coupling capacitance is 40 fF. The calculated results and the experimental data show an agreement on the main features of the waveforms. As the pulse propagates downstream, the high-frequency components attenuate strongly, causing an increase in the rise time. Similar observations on microstrip lines [11] and coplanar striplines [9] have been reported. In our case, the effect is more significant because of the additional reflections at the periodic sampling gaps, which screen away the high-frequency components. A good match between the theory and the experiment is also obtained on the broadening of pulse width and the reduction in peak amplitude relative to the tail. Minor differences between the curves can be attributed to back-plane reflection of the signals [13], which have not been included in the model.

To study in more detail the effect of periodic loading on signal propagation, a series of correlation curves are calculated using the coupling capacitance as a parameter (Fig. 7). The initial pulse and the propagation parameters are the same as those in Fig. 6(b). The propagation distance is taken to be 4 mm. The oscillations immediately following the main peaks are caused by modal dispersion. They appear because the low-frequency components propagate faster and "catch up" with the high-frequency components. When the capacitance is small, the multiple reflections are weak and are hardly observed. The effect becomes stronger as the capacitance increases. As a result, the high-frequency components in the main peak and in the oscillations are reduced. Another feature to be noticed is the appearance of a subsidiary peak on the tail caused by the reflections. With a further increase of the capacitance, an overall broadening in the trailing part of the curve is observed.

V. Conclusions

We have presented experimental data and theoretical work on the propagation of picosecond electrical pulses on a periodically loaded coplanar waveguide. The results show that multiple reflections of the signal among the sampling channels constitute an important factor in determining the pulse waveform. They lead to a reduction in the amplitudes of the high-frequency components and cause an additional broadening of the pulse.

Acknowledgment

The authors would like to thank L. Xu for helpful discussions and B. B. Hu for technical assistance in the work.

REFERENCES

[1] D. H. Auston, A. M. Johnson, P. R. Smith, and J. C. Bean, "Picosecond optoelectronic detection, sampling, and correlation measurements in amorphous semiconductors," *Appl. Phys. Lett.*, vol. 37, pp. 371–373, 1980.

[2] M. B. Ketchen *et al.*, "Generation of subpicosecond electrical pulses on coplanar transmission line," *Appl. Phys. Lett.*, vol. 48, pp. 751–753, 1986.

[3] F. W. Smith *et al.*, "Picosecond GaAs-based photoconductive optoelectronic detectors," *Appl. Phys. Lett.*, vol. 54, pp. 890–892, 1989.

[4] J. D. Morse, R. Mariella, G. D. Anderson, and R. W. Dutton, "Picosecond GaAs photoconductors on silicon substrates for local integration with silicon devices and circuits," *IEEE Electron Device Lett.*, vol. 10, pp. 7–10, 1989.

[5] H-L. A. Hung *et al.*, "Millimeter-wave monolithic integrated circuit characterization by a picosecond optoelectronic technique," *IEEE Trans. Microwave Theory Tech.*, vol. 37, pp. 1223–1231, 1989.

[6] K. K. Li, G. Arjavalingam, A. Dienes, and J. R. Whinnery, "Propagation of picosecond pulses on microwave striplines," *IEEE Trans. Microwave Theory Tech.*, vol. MTT-30, pp. 1270–1273, 1982.

[7] D. H. Auston, "Impulse response of photoconductors in transmission lines," *IEEE J. Quantum Electron.*, vol. QE-19, pp. 639–648, 1983.

[8] G. Hasnain, A. Dienes, and J. R. Whinnery, "Dispersion of picosecond pulses in coplanar transmission lines," *IEEE Trans. Microwave Theory Tech.*, vol. MTT-34, pp. 738–741, 1986.

[9] T. Y. Hsiang, J. F. Whitaker, R. Sobolewski, D. R. Dykaar, and G. A. Mourou, "Propagation characteristics of picosecond electrical transients on coplanar striplines," *Appl. Phys. Lett.*, vol. 51, pp. 1551–1553, 1987.

[10] D. E. Cooper, "Picosecond optoelectronic measurement of microstrip dispersion," *Appl. Phys. Lett.*, vol. 47, pp. 33–35, 1985.

[11] J. F. Whitaker, T. B. Norris, G. Mourou, and T. Y. Hsiang, "Pulse dispersion and shaping in microstrip lines," *IEEE Trans. Microwave Theory Tech.*, vol. MTT-35, pp. 41–47, 1986.

[12] D. R. Bowman, R. B. Hammond, and R. W. Dutton, "Polycrystalline-silicon integrated photoconductors for picosecond pulsing and gating," *IEEE Electron Device Lett.*, vol. EDL-6, pp. 502–504, 1985.

[13] N. G. Paulter and R. B. Hammond, "Photoconductor pulse generators and sampling gates for characterization of high-speed devices and transmission lines," *SPIE*, vol. 795, pp. 214–224, 1987.

[14] C. Shu and E. S. Yang, "100 GHz optoelectronic time division demultiplexing," Tech. Rep. (unpublished).

[15] E. Yamashita, K. Atsuki, and T. Ueda, "An approximate dispersion formula of microstrip lines for computer-aided design of microwave integrated circuits," *IEEE Trans. Microwave Theory Tech.*, vol. MTT-27, pp. 1036–1038, 1979.

[16] K. C. Gupta, R. Garg, and I. J. Bahl, *Microstrip Lines and Slotlines*. Norwood, MA: Artech House, 1979.

[17] D. B. Rutledge, D. P. Neikirk and D. P. Kasilingam, "Integrated-circuit antennas," in *Infrared and Millimeter Waves*, vol. 10, K. J. Button, Ed. New York: Academic Press, 1983.

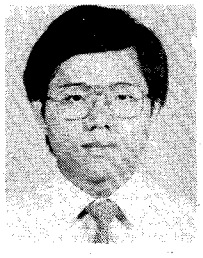

Chester Shu was born in Hong Kong in 1963. He received the B.Sc. degree in physics from the University of Hong Kong in 1985 and the M.S. degree in applied physics from Columbia University, New York NY, in 1986. He is currently working towards the Ph.D. degree at Columbia.

He worked at the Siemens Corporate Research Laboratories, Princeton, NJ, in the summer of 1988, where he was involved in the design and characterization of multiple quantum well lasers. His research interests include the fabrication and characterization of optoelectronic devices, the generation and detection of broad-band electrical pulses by picosecond optoelectronic technique, optical characterization of semiconductor materials, and high-T_c superconducting thin films.

Mr. Shu is a member of Sigma Xi and the American Physical Society.

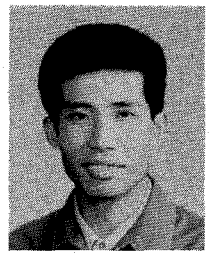

Xu Wu was born in Shanghai, China. He received the B.S. degree in physics from Fudan University, China, in 1982 and the M.A. degree, also in physics, from the University of Rochester, Rochester, NY, in 1983. He received the Ph.D. degree in electrical engineering from Columbia University, New York, NY, in 1987 and subsequently worked there as an Associate Research Scientist.

His research involves metal–semiconductor interface properties and microelectronic devices including high-speed heterostructure bipolar transistor and high-T_c superconducting films. Dr. Wu is currently a Research Scientist at Schlumberger-Doll Research, Ridgefield, CT, and is a member of the American Physical Society.

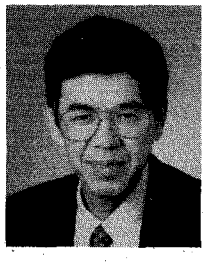

Edward S. Yang (S'60–M'61–SM'74) received the B.S. degree from Cheng-Kung University, Taiwan, the M.S. degree from Oklahoma State University, and the Ph.D. degree from Yale University.

He was with IBM in Poughkeepsie, NY, from 1961 to 1963. Since 1965, he has been a faculty member of the Electrical Engineering Department at Columbia University, New York, NY. He served as the Chairman of the department from 1987 to 1990. His earlier research work included electronics and optoelectronic devices. Recently, he has been involved in studies of silicon–germanium heterostructures, high-speed photodetectors, high-T_c superconducting films, polyemitter contacts, heterojunction bipolar transistors, physics in silicide–silicon interfaces, and metal GaAs Schottky barriers.

Dr. Yang is the author of two texts, *Fundamentals of Semiconductor Devices* (1978) and *Microelectronics Devices* (1988).

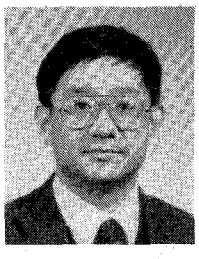

Xi-Cheng Zhang was born in Beijing, China, in 1956. He received the B.S. degree in physics from Peking University, China, in 1981 and the M.S. and Ph.D degrees in physics from Brown University, Providence, RI, in 1983 and 1986.

He was a visiting scientist at MIT in 1985. From 1985 to 1987, he worked in the Physical Technology Division, Amoco Research Center, Naperville, IL. In 1987, he joined the Department of Electrical Engineering, Columbia University, New York, NY. His research areas include optical characterization of semiconductor materials and their superlattice structures; high-speed electro-optic sampling; generation and detection of THz bandwidth electromagnetic radiation, and ultrafast optoelectronic devices for optical computing.

Dr. Zhang is the author of one textbook and more than 40 journal papers. He is a member of the American Physical Society.

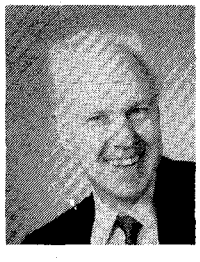

David H. Auston (S'67–M'69–SM'87–F'89) was born in Toronto, Canada. He received the Ph.D. degree from the University of California at Berkeley in 1969 and the B.A.Sc. and M.A.Sc. degrees from the University of Toronto in 1962 and 1963.

In 1969 he joined the technical staff of AT&T Bell Laboratories, Murray Hill, NJ, where he began research on high-speed optics and electronics. In 1982, he became Head of the High Speed Materials and Phenomena Department

in the Physics Division. He left Bell Laboratories and became Professor of Electrical Engineering and Applied Physics at Columbia University, New York, NY, in 1987. He became Chairman of the department in 1990 and Dean of the School of Engineering and Applied Science in 1991. At Columbia University, Dr. Auston continued his research on the development of novel high-speed measurement techniques.

Dr. Auston is a Fellow of the Optical Society of America and the American Physical Society. He is also a member of the National Academy of Engineering. In 1985, he received the R. W. Wood prize of the Optical Society of America. In 1990, he was awarded the Quantum Electronics Award of the Lasers and Electro-optics Society of the IEEE, and in 1991, he will receive the Morris E. Leeds Award of the IEEE.